Asian Journal of Civil Engineering (2023) 24:3893–3905
https://doi.org/10.1007/s42107-023-00705-2

METHODOLOGY

Pressure-impulse diagrams using coupled single degree of freedom systems subjected to blast load

Anita Bhatt[1] · **Pradeep Bhargava**[1]

Received: 5 May 2023 / Accepted: 8 May 2023 / Published online: 16 May 2023

Abstract

Pressure-Impulse (P-I) diagrams, a widely popularized approach, relate different damage levels and are utilized in the preliminary design of structural elements subjected to blast loading. In the presented paper, P-I diagrams generated using coupled Single Degree of Freedom (SDOF) model subjected to blast loading are studied. It may be noted that these P-I diagrams for the blast in the dynamic and impulsive regime are very different from those derived by applying the uncoupled SDOF approach. The resultant P-I diagrams are further compared with those based on Timoshenko beam theory, including the higher modes effect. The findings are intended to shed light on how to develop simpler, more accurate methods for calculating the combined reaction of structural parts exposed to various blast loading ranges. The effect of shear and flexure resistance ratio on P-I diagrams has been studied parametrically. P-I diagrams show only small fluctuations as they approach quasi-static regimes, indicating that they are not sensitive to the shear and flexure resistance ratio for a distant range of blast loadings.

Keywords Distant blast · Flexibility · Higher modes · Pressure-impulse curve · Timoshenko beam

Introduction

The dynamic response of structural elements under blast loading can be represented in various forms. Single degree of freedom (SDOF) models, due to their simplicity, are widely employed strategies that several researchers adopt to predict the dynamic response (Biggs, 1964; Smith & Hetherington, 1994Defense UFC, 2008). Numerical methods used in a variety of methods accurately represent the structural elements' dynamic response exposed to blast load (Jayasooriya, 2010). FEM software like Abaqus, LS Dyna, etc., have been used to simulate the problem by several investigators (Ibrahim et al., 2017; Jayasooriya, 2010; Kadid, 2008), but it consumes a lot of computational time. P-I (Pressure-impulse) diagrams are one of the most popularized and efficient tools to examine the damage of structural elements subjected to blast loading (Fallah & Louca, 2007; Syed et al., 2014). A significant amount of work on the generation of pressure-impulse diagrams has been done by number of researchers. The pressure-impulse diagrams can be generated through experiments (Liu et al., 2018), numerical simulations, and theoretical calculations (Dragos & Wu, 2014; Fallah & Louca, 2007; Youngdahl, 1970).

The pressure impulse diagrams paradigm was conceived in the mid-1950s. Much of the study generally assume the damage is usually linked to the flexure response on the basis of Biggs' method defining flexural resistance function as elastic-rigid plastic, elastic, elastic–plastic softening, and hardening (Biggs, 1964; Fallah & Louca, 2007; Gantes & Pnevmatikos, 2004; Smith & Hetherington, 1994). May and Smith introduced the SDOF approach for structural materials exposed to blast loads on the basis of the ratio of the load duration to the time period of the comparable SDOF, namely, impulsive and dynamic (Smith & Hetherington, 1994). Researchers (Gantes & Pnevmatikos, 2004) described the response spectrum on the basis of exponential blast pressure distribution taking into account the material's elastic–plastic nature. Pressure-impulse diagrams in form of three regimes on the basis of the positive pulse duration of the load and the natural period of the structure has been suggested by Cormie et al. (2009). To create the iso-damage diagram with elastic–plastic hardening and elastic–plastic softening under blast loading, Fallah and Louca analyzed the SDOF systems (Fallah & Louca, 2007). The reaction was split into

✉ Anita Bhatt
abhatt@ce.iitr.ac.in

[1] Department of Civil Engineering, IIT Roorkee, Roorkee 247667, India

elastic, rigid-plastic-hardening/ softening, elastic–plastic-hardening and softening categories using dimensionless parameters. In order to generalize the system's solution, inverse ductility, and softening/ hardening indices were included as dimensionless parameters. Youngdahl (1970) and Li and Meng (2002) and others discussed the impact of impulse loading shape on an elastic–plastic SDOF system's dynamic response. The situation was divided into elastic–plastic, elastic, and rigid-plastic structural responses using two dimensionless factors. To provide each response category with a distinct loading shape and separate P-I diagram, dimensionless parameters were introduced. Campidelli and Voila (2007) pointed out that equations proposed by Li and Meng (2002) need modification for some complex pulse shapes.

Several mechanisms can cause a flexural member to fail (i.e., flexure, shear, combined failure) when subjected to varying range of blast scenario (Slawson, 1984). Direct shear failure modes and flexure failure modes are always independent of one another, according to Krauthammer et al. (2008). The P-I diagram, which is made up of two threshold curves that each reflect a failure mode corresponding to direct shear and flexure, has two failure modes, according to Krauthammer (2008). In the numerical simulation conducted by Mutalib and Hao (2013), the authors recognized three primary damage modes of Reinforced Concrete (RC) columns. In the study of Ma et al. (2012), the evaluation of the failure mode categories for fully clamped and simply supported beams has been explored. In the authors' research, the bending and shear failures were evaluated, and the responses of the beams using five transverse velocity profiles were investigated. Three failure mechanisms were explored by Ma et al. (2012). Only shear is present in mode 1. The element's plastic hinge in the element's centre serves as the mode 2, indicator for the bending failure. Mode 3 is feasible to recognize as the confluence of mode 1 and mode 2. To simulate the interdependence of the flexure and direct shear modes of failure, Dragos et al. (2014) conducted a 1-D FEM analysis. The authors performed a parametric analysis to better understand how the flexure and direct shear response interact and exhibited the flexure member reaction during the direct shear response. Runquin Yu et al. (2018) produced non-dimensional pressure impulse diagrams based on Euler Bernoulli's theory to predict combined response.

In the present work, a forecast of the dynamic response of the reinforced concrete flexural components in different explosion ranges was conducted in the form of P-I diagram. The response expressed in form of (P-I) diagrams were created with the help of a coupled SDOF model that takes into account the interaction between flexure and shear responses. The resultant pressure-impulse diagrams are compared with traditional P-I diagrams on the basis of the uncoupled SDOF model. P-I diagrams are also contrasted with Timoshenko beam theory- based diagrams that take higher mode impact into account.

Pressure impulse diagrams for coupled SDOF system

Pressure impulse diagrams

The standardized P-I characteristics of the blast loading, which may apply to any given blast scenario, are one of the approach to depict the structure's dynamic response under the blast load (Abedini et al., 2019). To achieve a distinct amount of predetermined damage for the structures under consideration, pressure impulse diagrams are an appropriate approach to link blast pressure duration and amplitude (Van der Meer et al., 2010). The impulsive, dynamic, as well as quasi-static loading regimes could be utilized to segment a pressure impulse (P-I) curve (Syed et al., 2014). The applied pressure (quasi-static area), impulse (impulsive area), or both the applied impulse & pressure (dynamic regime) may completely determine the structural element's maximal response (Bhatt et al., 2021). A short- duration dynamic load serves as a representation of the impulsive case. In this loading scenario, the structure under examination does not respond to its maximum response until after the load duration has passed. The maximal response of the structure is attained close to the end of the loading regime since the dynamic regime is represented by a dynamic load. The quasi-static regime illustrates the scenario of dynamic load when maximal structural response is attained before the applied load is removed. Figure 1 depicts the key properties of the P-I curve (Bhatt et al., 2021).

Both the pressure and the impulsive asymptote may be used to classify the P-I diagram. The impulsive asymptote is connected to an extremely dynamic load of very short duration in comparision to the structure's naturally occurring period, which is controlled by impulse. The pressure asymptote, on the other hand, is connected to a longer-lasting dynamic loading and thus susceptible to a quasi-static load condition controlled by pressure.

The present study employs the Coupled Single Degree of Freedom (CSDOF) approach model proposed by Bhatt et al., (2023, under communication) to incorporate the direct coupling between direct shear-slip and flexure response and the SDOF model (Bhatt et al., 2021) based on Timoshenko beam theory, including higher modes, to forecast the pressure-impulse diagrams. Specifics of the adopted approach are discussed in subsequent sections.

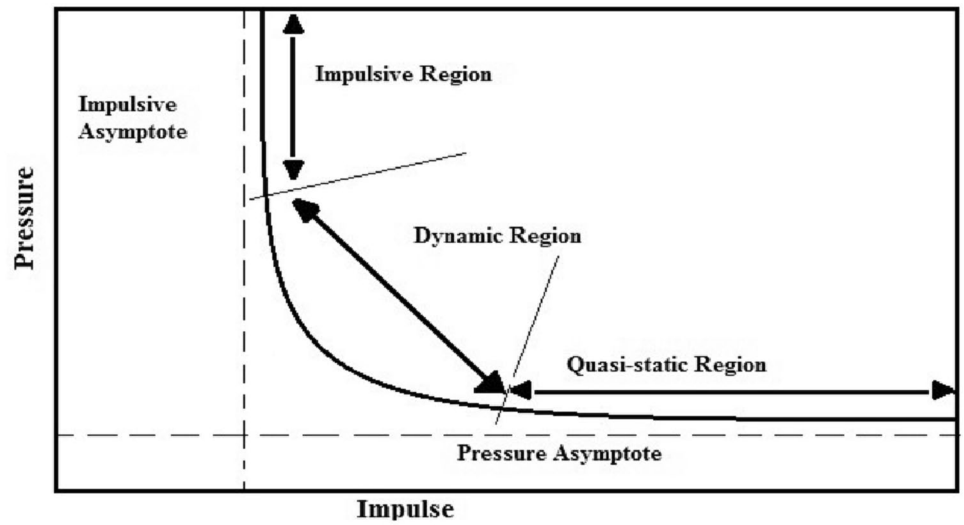

Fig. 1 Pressure-Impulse diagram (after, Bhatt et al., 2021)

Coupled single degree of freedom (CSDOF) system model (Bhatt et al., 2023, under communication)

The present work employs Coupled SDOF system model (Bhatt et al., 2023, under communication) to generate pressure-impulse (P-I) curves for structural elements under consideration. When exposed to a variety of blast loads, the majority of structural components with suitable flexure and shear capacity often exhibit combined shear-flexure deformation mode. The system's shear and flexure resistance will determine the deformation modes, such as direct shear-slip at support and flexure failure at the center, thus they shouldn't be handled separately. Based on several studies, Fig. 2 depicts the assumed deflected profile that a beam could experience when exposed to blast load (Bhatt et al., 2023; Jones & Alves, 2004; Ross, 1986; Slawson, 1984; Xu et al., 2014; Zhang et al., 2019).

Idealizing a system as an equivalent Single Degree of Freedom (SDOF) system, which is defined by the following equation of motion, is a frequently used method for analyzing a system's dynamic response. The following is a notation for the governing equation of motion:

$$k_m M\ddot{y}(t) + k_l K y(t) = k_l P(t) \quad (1)$$

Or alternatively,

$$k_{ml} M\ddot{y}(t) + K y(t) = P(t) \text{where, } k_{ml} = \frac{k_m}{k_l} \quad (2)$$

where M is the total mass of the system, k_m is a corresponding equivalent mass factor, K is the stiffness, k_l is equivalent load factor, and $y(t)$and$\ddot{y}(t)$ are dynamic transverse displacement and acceleration response, respectively and $P(t)$is equivalent blast load (P(t) = b × L × p(t)), where the load pressure can be given as:

$$p(t) = p_o\left(1 - \frac{t}{t_d}\right), t < t_d = 0, t \geq t_d \quad (3)$$

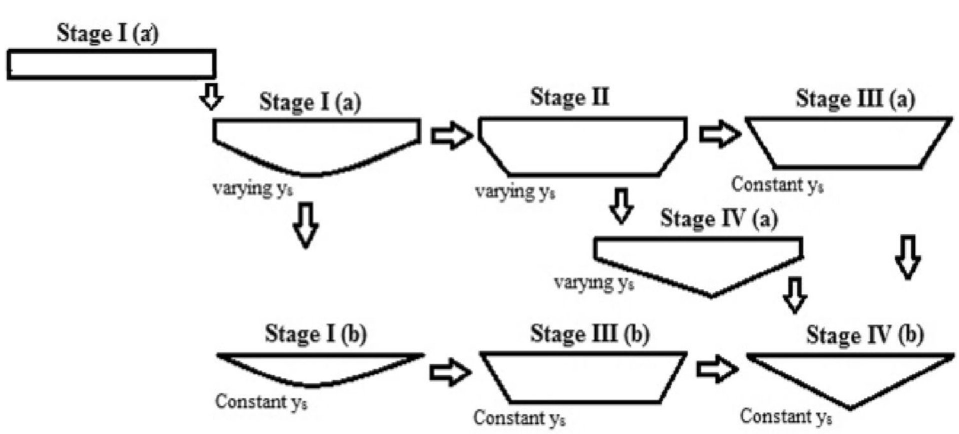

Fig. 2 Deflected shape profile for combined shear-flexure failure (after Bhatt et al., 2023, under communication)

A simplified triangular pulse closely approximates the real impulsive blast load neglecting the negative load phase (Biggs, 1964).

The present section provides the conceptual background to coupled SDOF system's equation of motions for all the deformation modes listed (as illustrated in Fig. 2). Accordingly, flexure response combined with support slip for the RC beam can be categorized into stages as given subsequently:

Stage I (a')–Direct shear response (with varying support slip)

The direct shear response involves the rigid body translation of member, depending on the slip at the support, y_s (Fig. 3). During this stage the flexure resistance mechanism has yet not initiated, and the structural member has not yet undergone the flexure deformation (after Bhatt et al., 2023, under communication).

The dynamic force equilibrium equation for the system may be expressed as:

$$0 = \int_0^l -p(t)dx + \int_0^l m\ddot{y}_s(t)dx + V_s \tag{4}$$

which, in turn, may be simplified in the form of SDOF system equation of motion as:

$$M\ddot{y}_s + V(t) = P(t) \tag{5}$$

where $V(t)$ is the shear resistance function mobilized corresponding to the support slip y_s.

Stage I (a)-Elastic response (along with varying support slip):

Initially, the assumption taken is that shear resistance and flexure resistance is within the elastic limit.

The assumed profile of elastic deflected shape, in terms of mid-span deflection y_m and support slip y_s, is represented as (Fig. 4):

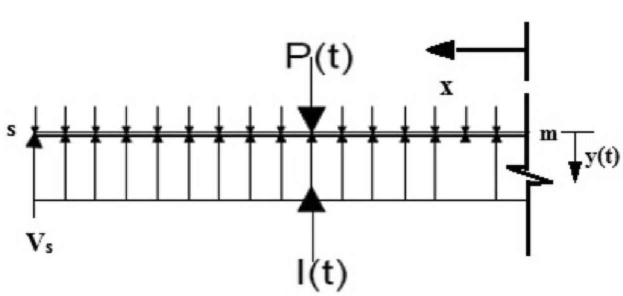

Fig. 3 Direct shear response mode (after Bhatt et al., 2023, under communication)

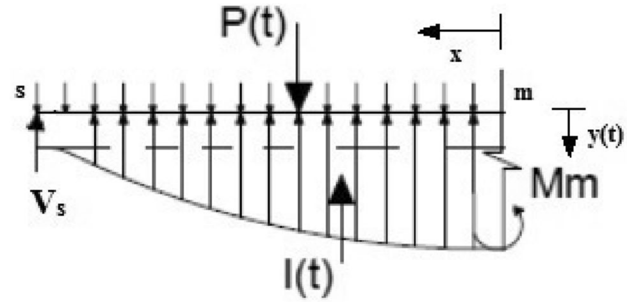

Fig. 4 Combined shear-elastic flexure failure mode (after Bhatt et al., 2023, under communication)

$$Y(x,t) = \left(y_m(t) - y_s(t)\right)\left(\cos\left(\frac{\pi x}{2l}\right)\right) + y_s(t), x\,\forall\, 0\ to\ l \tag{6}$$

Dynamic rotational and force equilibrium equations may be written as:

$$0 = -\frac{p(t)l^2}{2} + \left(\ddot{y}_m(t) - \ddot{y}_s(t)\right)\int_0^l m\left(\cos\left(\frac{\pi x}{2l}\right)\right)(l-x)dx + \ddot{y}_s(t)\frac{ml^2}{2} + M_m \tag{7}$$

$$0 = -p(t)l + \left(\ddot{y}_m(t) - \ddot{y}_s(t)\right)\int_0^l m\left(\cos\left(\frac{\pi x}{2l}\right)\right)dx + ml\ddot{y}_s(t) + V_s \tag{8}$$

which, in turn, combined with Eq. (6), yields SDOF equation at mid-span and support as:

$$\text{Mid} - \text{span}: (t) + 2.0885Ky_m(t) - 1.0885V(t) = P(t) \tag{9}$$

$$\text{Support}: M\ddot{y}_s(t) - 3.6586Ky_s(t) + 4.6586V(t) = P(t) \tag{10}$$

It may be emphasized that both resistance functions, moment $M_m = \beta_1 M_o, \beta_1 < 1$ and shear $V(t) = \beta_2 V_o, \beta_2 < 1$, are within the elastic range.

Stage I (b)–Elastic response with constant support slip:

At stage I (b), the support slip attains a constant value, albeit within the elastic limit. This scenario can be observed in the case of the distant blast (lower magnitude). In this stage, after attaining a certain amount of slip, flexure mode dominates the response of the structural element (Fig. 5).

$$Y(x,t) = y_m(t)\left(\cos\left(\frac{\pi x}{2l}\right)\right), x\,\forall\, 0\ to\ l \tag{11}$$

The dynamic rotational equilibrium equation is written as:

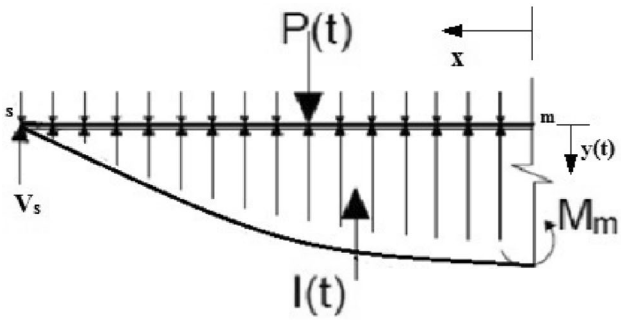

Fig. 5 The elastic flexure failure mode for simply supported beam (after Bhatt et al., 2023, under communication)

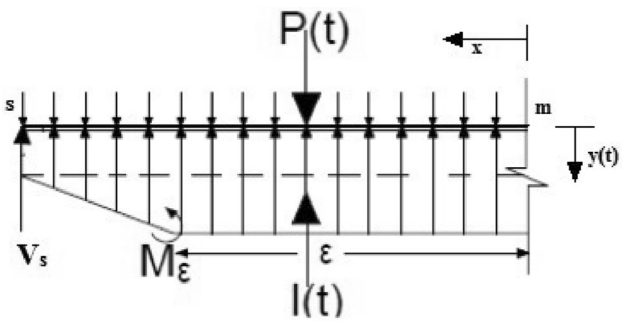

Fig. 6 Combined shear-plastic flexure failure mode with hinge propagation (after Bhatt et al., 2023, under communication)

$$0 = \int_0^l -p(t)(l-x)dx + \int_0^l m\ddot{Y}(x,t)(l-x)dx + M_m \tag{12}$$

Considering Eqs. (11) and (12), the SDOF system's equation of motion becomes:

$$k_{ml}M\ddot{y}_m(t) + Ky_m(t) = P(t), k_{ml} = 0.8 \tag{13}$$

where y_m is the mid-node transverse dynamic deflection,$M_m = \beta_1 M_o, \beta_1 < 1$ is the moment resistance offered by the beam at the center, and M_o is moment capacity of the section.

Stage II–Dynamic plastic response along with a varying slip:

The structure experiences both support slip and flexure deformations. The flexure resistance has reached the plastic region. This condition is observed in the case of the near blast. The assumption is that the hinge zone will not propagate towards the mid-span of the beam until slip is taking place at support (Abedini et al., 2013; Jones & Alves, 2004).

The assumed profile of dynamic plastic deflected shape is represented as (Fig. 6)

$$Y(x,t) = y_m(t), x\,\forall 0\; to\; \varepsilon^-, \varepsilon^- = \varepsilon - \delta x, \delta x \to 0 \tag{14}$$

$$\begin{aligned} Y(x,t) = {} & (y_\varepsilon(t) - y_s(t))\frac{l-x}{l-\varepsilon} + y_s(t), x\forall\varepsilon^+ tol, \varepsilon^+ \\ & = \varepsilon + \delta x, \delta x \to 0 \end{aligned} \tag{15}$$

Once again, the dynamic rotational and force equilibrium may be written as:

$$\begin{aligned} 0 = {} & -p(t)\varepsilon\left(l - \frac{\varepsilon}{2}\right)\Big|_0^{\varepsilon^-} + m\ddot{y}_m(t)\varepsilon\left(l - \frac{\varepsilon}{2}\right)\Big|_0^{\varepsilon^-} \\ & - p(t)\frac{(l-\varepsilon)^2}{2}\Big|_{\varepsilon^+}^l + m\big(\ddot{y}_\varepsilon(t) - \ddot{y}_s(t)\big)\frac{(l-\varepsilon)^2}{3}\Big|_{\varepsilon^+}^l \\ & + m\ddot{y}_s(t))\frac{(l-\varepsilon)^2}{2}\Big|_{\varepsilon^+}^l + M_{\varepsilon^+} \end{aligned} \tag{16}$$

$$\begin{aligned} 0 = {} & -p(t)\varepsilon\big|_0^{\varepsilon^-} + m\ddot{y}_m(t)\varepsilon\big|_0^{\varepsilon^-} - p(t)(l-\varepsilon)\big|_{\varepsilon^+}^l \\ & + m\big(\ddot{y}_\varepsilon(t) - \ddot{y}_s(t)\big)\frac{(l-\varepsilon)}{2}\Big|_{\varepsilon^+}^l + m\ddot{y}_s(t)(l-\varepsilon)\big|_{\varepsilon^+}^l + V(t)_s \end{aligned} \tag{17}$$

Combining Eqs. (14) and (15) with (16) and (17), the equation of motion for the SDOF system can be re-cast as:

Dynamic plastic zone:

$$M\ddot{y}_m(t) = P(t) \tag{18}$$

Beyond the dynamic plastic zone ($x > \varepsilon$):

$$M\ddot{y}_\varepsilon(t) + \frac{3l^2}{(l-\varepsilon)^2}R_m - \frac{2l}{l-\varepsilon}V(t) = P(t) \tag{19}$$

Support:

$$M\ddot{y}_s(t) - \frac{3l^2}{(l-\varepsilon)^2}R_m + \frac{4l}{l-\varepsilon}V(t) = P(t) \tag{20}$$

Stage III–Dynamic plastic deformation with a constant support slip:

At this stage, the slip has attained its maximum value, flexure resistance has reached the plastic region, and the hinge zone starts propagating towards the mid-span of the beam.

Assuming the dynamic plastic zone extending to a length ε as shown in Fig. 7, the deflected shape can be represented as-

$$Y(x,t) = y_m(t), x\,\forall 0\; to\; \varepsilon^-, \varepsilon^- = \varepsilon - \delta x, \delta x \to 0 \tag{21}$$

$$Y(x,t) = y_\varepsilon(t)\frac{l-x}{l-\varepsilon}, x\forall\varepsilon^+ tol, \varepsilon^+ = \varepsilon + \delta x, \delta x \to 0 \tag{22}$$

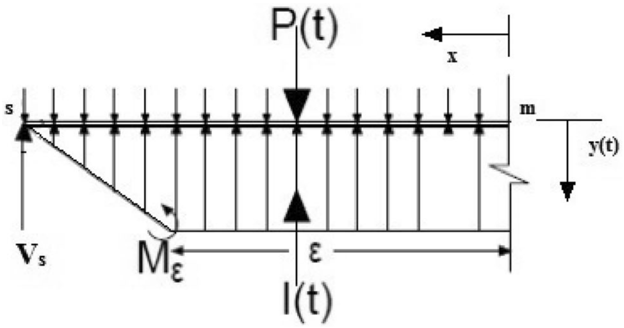

Fig. 7 Plastic flexure failure mode with propagating hinge (after Bhatt et al., 2023, under communication)

The dynamic rotational equilibrium equation may be derived as:

$$0=\int_0^l -p(t)(l-x)dx+\int_0^l m\ddot{Y}(x,t)(l-x)dx+M_{\varepsilon^+} \quad (23)$$

$$0=-p(t)\varepsilon\left(l-\frac{\varepsilon}{2}\right)|_0^{\varepsilon^-}+m\ddot{y}_m(t)\varepsilon\left(l-\frac{\varepsilon}{2}\right)|_0^{\varepsilon^-} -p(t)\frac{(l-\varepsilon)^2}{2}|_{\varepsilon^+}^l+m\ddot{y}_\varepsilon(t)\left(\frac{l-\varepsilon}{2}\right)^2|_{\varepsilon^+}^l+M_{|\varepsilon^+} \quad (24)$$

In the dynamic hinge zone, the external load is fully resisted by inertial force as the moment resistance diminishes. However, for the section beyond the plastic zone, moment resistance is a part of the equilibrium equation with $M_{|\varepsilon^+}=M_o$ (Jones & Alves, 2004). Equations (23) and (24) can be easily re-expressed as:

For dynamic plastic zone:

$$M\ddot{y}_m(t)=P(t) \quad (25)$$

Beyond dynamic plastic zone ($x>\varepsilon$):

$$\frac{2}{3}M\ddot{y}_\varepsilon(t)+\frac{l^2}{(l-\varepsilon)^2}R_m=P(t) \quad (26)$$

Stage IV (a)–Static plastic deformation along with varying support slip:

The hinge forms at the mid-span of the beam along with a direct shear-slip at support.

Assuming deflected profile for static plastic response is given as (Fig. 8):

$$Y(x,t)=(y_m(t)-y_s(t))\frac{l-x}{l}+y_s(t), x\forall 0\ to\ l \quad (27)$$

The dynamic rotational and force equilibrium may be written as:

$$0=-p(t)\frac{l^2}{2}|_0^l+m(\ddot{y}_m(t)-\ddot{y}_s(t))\frac{l^2}{3}|_0^l+m\ddot{y}_s(t)\frac{l^2}{2}|_0^l+M_m \quad (28)$$

$$0=-p(t)l|_0^l+m(\ddot{y}_m(t)-\ddot{y}_s(t))\frac{l}{2}|_0^l+m\ddot{y}_s(t)l|_0^l+V_s \quad (29)$$

Combining Eqs. (28) and (29) with Eq. (27), the equation of motion for the SDOF system can be written as:

$$\text{Mid}-\ddot{\text{s}}\text{pan}: y_m(t)+3R_m-2V(t)=P(t) \quad (30)$$

$$\text{Support}: M\ddot{y}_s(t)-3R_m+4V(t)=P(t) \quad (31)$$

Stage IV (b)–Static plastic deformation with constant support slip:

Assuming the profile for static plastic deflected shape as (Fig. 9):

$$Y(x,t)=y_m(t)\frac{l-x}{l}, x\forall 0\ to\ l \quad (32)$$

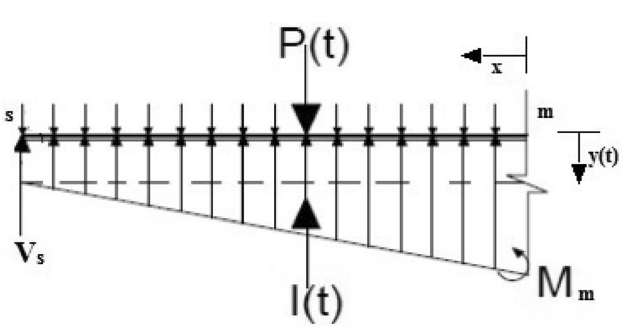

Fig. 8 Combined shear-plastic flexure failure mode with a hinge at mid-span of a beam (after Bhatt et al., 2023, under communication)

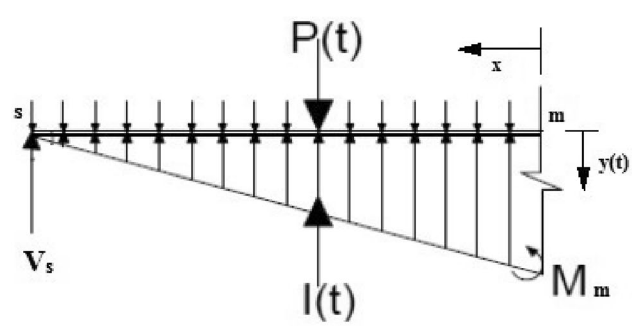

Fig. 9 Plastic flexure failure mode with a hinge at mid-span of a beam (after Bhatt et al., 2023, under communication)

The dynamic rotational equilibrium for the system is written as:

$$0=\int_0^l -p(t)(l-x)dx+\int_0^l m\ddot{Y}(x,t)(l-x)dx+M_m,\ M_m=M_o \quad (33)$$

Alternatively, it may be written in the form of SDOF system:

$$M\ddot{y}(t)+\frac{2}{3}R_m=P(t) \quad (34)$$

SDOF model including higher modes (Bhatt et al., 2021)

The frequency and mode shape of a transversely vibrating beam

Each system's mode shape and natural frequency are determined by the system's material and geometrical features. In Eqs. (35), (36), the following parameters are (Han et al., 1999):

$$Geometry\,parameter, s=L\sqrt{\frac{A}{I}} \quad (35)$$

$$Material\,parameter, \gamma=\sqrt{\frac{E}{G}} \quad (36)$$

where E indicates Young's modulus, G signifies shear modulus, I represents the second moment of the cross-section area of the beam, and A signifies a cross-section area of the beam.

The wave numbers denoted as a_n and b_n, are utilized to produce the formulation for the mode shape of structural components, which results in the solution of the frequency equation. These wave numbers rely on s and γ and are established parameters for structural components.

These frequency equations are controlled by the transversely vibrating boundary conditions. The appropriate frequency eq. and mode shape for the simply supported boundary-conditioned beam are shown in Table 1.

Using the aforementioned Eqs. (35) and (36), the mode shapes may be obtained once s and γ have been evaluated for structural elements. The ortho-normalization eq. of the beam's mode shapes is employed to get the value of C_n, as shown in Table 2 below.

Table 1 Mode shape and frequency eq. for simply supported beam

S. no	Beam theory	Frequency equation	Mode shape
1	Timoshenko	$\sin(a*l)\sinh(b*l)=0$	$W_n(x)=C_n\{\sin(a*x)\}$

Table 2 Ortho-normalization equation for simply supported beam

S. no	Beam theory	Equation for ortho-normalizing
1	Timoshenko	$\int_0^l (W_n(x)\rho A W_m(x)+\varphi_n(x)\rho I\varphi_m(x))dx=\delta_{mn}$

The Kronecker delta, denoted by δ_{mn} is 1 when $n=m$ and 0 otherwise

The equation in Table 3 is used to calculate natural frequency.

Using mode superposition response of a transverse beam subjected to blast load (Chopra, 2012)

Both mode shape and fundamental frequencies of the structure under investigation are independent of imposed dynamic load and rely on the material and geometric characteristics. Yet, in addition to the imposed load, natural frequency and mode shape also affect a structure's dynamic response.

Let's assume that the load has a uniform distribution with a spatial distribution of p(x), and a temporal distribution of P(t).

$$\overline{p_n}=p_nL^3/EI \quad (37)$$

Here, p_n indicates uniformly distributed load and $\overline{p_n}$ represents dimensionless equivalent of load.

Every mode may be thought of as its own separate SDOF system. The SDOF system's natural frequency ω_n, the duration of the blast load t_d, and the pulse shape all affect the dynamic amplification factor $D_n(t)$.

The system's dynamic response in the n^{th} mode is a function of the time-dependent dynamic amplification factor $D_n(t)$, the mode shape $W_n(x)$ and the "modal participation" factor, which is

$$P_n=\int_0^l W_n(x)p(x)dx \quad (38)$$

The dynamic transverse displacement in the n^{th} mode examined by Chopra (2012) as

$$\overline{y_n}(x,t)=\frac{P_n}{\omega_n}D_n(t)W_n(x) \quad (39)$$

Table 3 Natural frequency for beam

S. no	Beam theory	Natural frequency
1	Timoshenko	$\omega_n=\frac{\sqrt{a_n^2-b_n^2}}{\sqrt{1+\gamma^2}}\sqrt{\frac{E}{\rho}}\frac{1}{L}$

Determination of pressure-impulse curve (iso-damage curve)

The maximum dynamic response obtained using elastic SDOF analysis can represent the required damage level (ductility ratio $\mu = 1$) and hence can be used as a governing parameter to obtain the Pressure-Impulse curve (iso-damage curve). The maximum dynamic response can be written as:

$$y_m = y_{st} D_{n,max} \tag{40}$$

where y_{st} is the static response and $D_{n,max}$ is the maximum time-dependent dynamic load amplification factor.

If the damage criterion is restricted to $y_m = y_c$, where y_c is the critical response, as proposed by Li and Meng (2002) dimensionless pressure-impulse curve can be obtained as:

$$\text{Pressure co-ordinate}: \frac{y_m}{y_c} = \frac{y_{st} D_{n,max}}{y_c} = 1 \rightarrow P = \frac{P_o}{K y_m} = \frac{y_{st}}{y_c} = \frac{1}{D_{n,max}} \tag{41}$$

$$\text{Impulse co-ordinate}: I = \frac{I}{y_m \sqrt{KM}} = \frac{p t_d}{2} = \frac{y_{st} \omega_n t_d}{2 y_c} = \frac{\omega_n t_d}{2 D_{n,max}} \tag{42}$$

Thus, obtaining values of maximum dynamic amplification for variable blast load cases, the Pressure Impulse curve can be plotted using the equations mentioned above.

Results and discussion

Validation of SDOF systems

The aforementioned CSDOF formulations in the proceeding section have been validated using experimental study on simply supported beam (Wu, 2012; Xu et al., 2014). The dynamic response predicted using the above two formulations and existing SDOF (Bigg/ Krauthammer) formulation is compared with limited experimental information available. The data regarding the geometric/ material properties of the beams and the blast load is summarized in Table 4 subsequently.

Frequencies are calculated and illustrated in Table 5 below for the above mentioned simply supported beam using Tables 1, 2, and 3.

The maximum deflection at mid-span and support experimentally measured and forecast using various SDOF models is shown in Table 6.

Table 4 Illustration of example under consideration

Properties of the beam			
Area moment of inertia (I)	0.000032 m^4	Poisson's ratio	0.2
Density (ρ)	2400 kg/m^3	Shear factor	0.822
Cross-sectional area (A)	0.04 m^2	Slenderness ratio	70.71
Length (L)	2.0 m	Young's modulus (E)	25.7 GPa
Modulus of rigidity (G)	12.5 GPa		
Blast loading charateristics			
Charge distance (m)	1.5	p_o (MPa)	12.42
Charge weight (TNT) (kg)	8.3	t_d (ms)	0.276

Pressure-impulse diagrams

Fourteen blast load scenarios emcompassing a range of the blast's intensity have been taken into consideration for the generation of the pressure-impulse diagrams. The near-blast load situation is susceptible to the impulsive asymptote (high peak pressure and short duration). In contrast, distant blast load instances with protracted duration

Table 5 Timoshenko's theory for simply supported beams is used to calculate the wave numbers and frequencies

Mode	Timoshenko			
n	Wave number a_n	Wave number b_n	Natural frequency ω_n	Ortho-normal Constant C_n
1	3.14	3.12	245.79	0.28
2	6.28	6.19	951.23	0.28
3	9.42	9.12	2103.44	0.29
4	12.56	11.88	3654.38	0.29
5	15.71	14.42	5554.24	0.29
6	18.85	16.73	7751.75	0.29
7	21.99	18.79	10.198.35	0.29
8	25.13	20.60	12.850.52	0.29

Table 6 Results and observations

Method	Flexural response		Direct shear response (Maximum support slip)
	Mid-span deflection	Rotation at the support	
Biggs'	42.0 mm	2.4°	–
Experimental	33.6 mm	–	–
Euler–Bernoulli (1 mode)	40.6 mm	–	–
Timoshenko (1 mode)	40.4 mm	2.89°	–
Coupled SDOF	35.8 mm	2°	–

and comparatively lower peak pressure are susceptible to quasi-static asymptote. Figure 10 displays pressure-impulse (iso-damage) diagrams predicted using Bigg's elastic SDOF model, SDOF model based on Timoshenko beam theory for 1 and 8 modes and coupled elastic SDOF model.

All of the aforementioned methods leads to convergence in the pressure-impulse diagrams for distant blast scenarios (quasi-static asymptote). While in the event of a near blast (Impulsive asymptote), pressure-impulse diagrams obtained using Bigg and Timoshenko mode 1 demonstrate convergence and pressure-impulse diagrams predicted using coupled SDOF model approaches that obtained using Timoshenko model including higher modes.

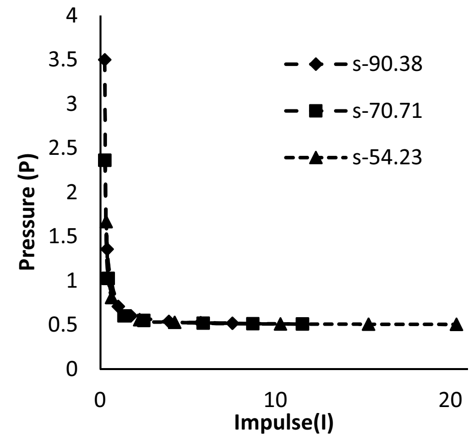

Fig. 11 Pressure-Impulse curve for various slenderness ratios using Timoshenko beam theory

Effect of flexibility

For employing beam theory to determine a structure's dynamic response subjected to blast load, flexibility plays a crucial role (Bhatt et al., 2021). Pressure-impulse diagrams are produced for three beams having different flexibility (slenderness ratio-90.38, 70.71, 54.23) by using Timoshenko beam theory considering the first 8 modes (represented using s) and elastic coupled SDOF system methodology

Fig. 10 A comparison of coupled SDOF dynamic regime of Pressure-Impulse diagram

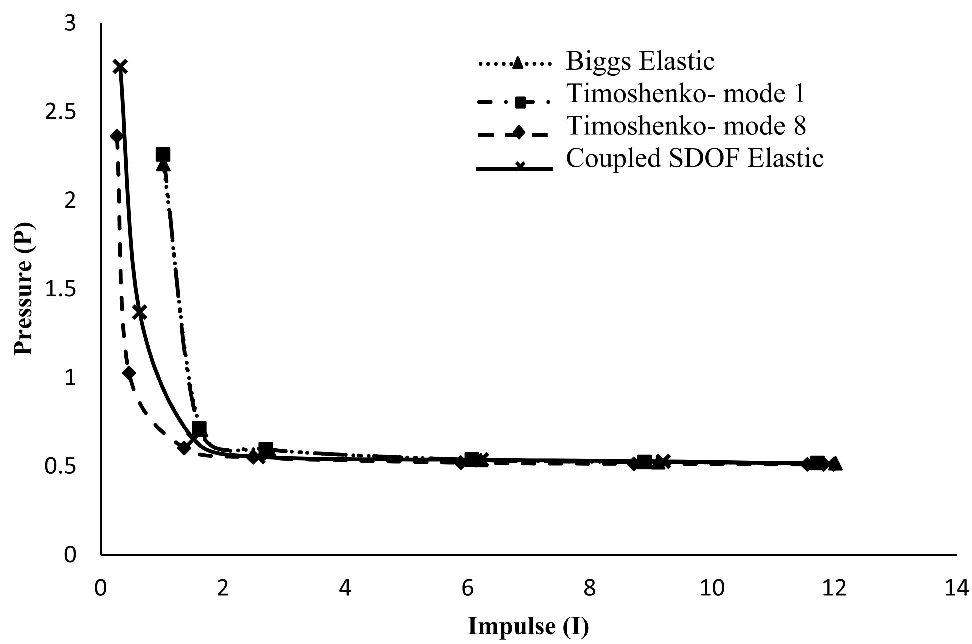

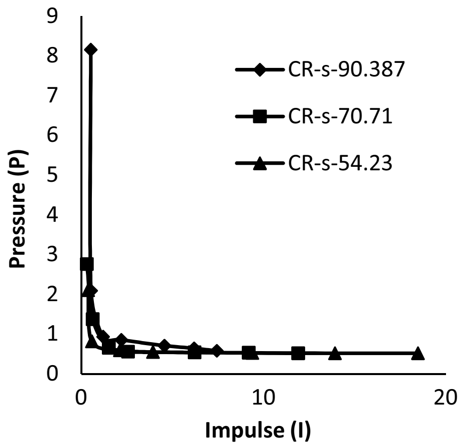

Fig. 12 Pressure-Impulse curve for various slenderness ratios using coupled SDOF system

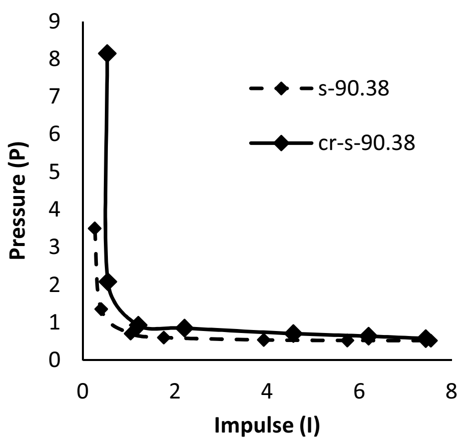

Fig. 13 Pressure-Impulse curve for slenderness ratio of 90.38

(represented using CR-s). The attempt is to capture the effect of flexibility on the structure's response subjected to a varying range of blast load. It is apparent from Figs. 11 and 12 that as the flexibility of the structural element decreases, the Pressure-Impulse diagram shifts towards a quasi-static regime, implying less severity towards blast loads.

Figure 13 shows Pressure-Impulse diagrams predicted for slenderness ratio 90.38 using the SDOF model based on Timoshenko beam theory including the first 8 modes and Coupled SDOF system. Both the diagrams slightly deviate for very near blast scenarios. The Timoshenko SDOF model shows an over-conservative response. Figure 14 shows Pressure-Impulse diagrams predicted for slenderness ratio 70.71 using the SDOF model based on Timoshenko beam theory including the first 8 modes and coupled SDOF system. Both the diagrams converge. Figure 15 shows Pressure-Impulse diagrams predicted for slenderness ratio 54.23 using SDOF model based on Timoshenko beam theory including the first

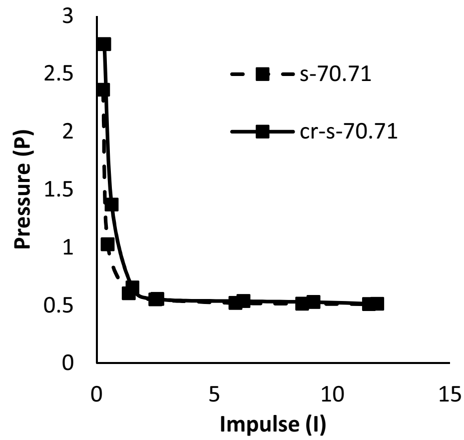

Fig. 14 Pressure-Impulse curve for slenderness ratio of 70.71

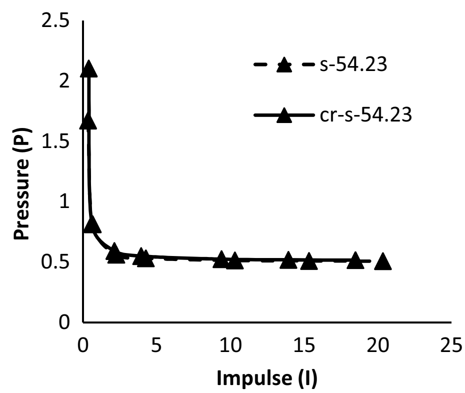

Fig. 15 Pressure-Impulse curve for slenderness ratio of 54.23

8 modes and coupled SDOF system. P-I diagram produced based on Timoshenko beam theory shifts towards the quasi-static regime.

Effect of shear capacity and flexure capacity ratio (V_o/ R_m)

Figure 16 shows Pressure-Impulse (iso-damage) diagrams predicted using Coupled elastic SDOF model for various V_o/R_m (i.e., 0.416, 1, 1.57, 2, 2.6). Figure 17 indicates the magnified dynamic regime of the P-I diagram shown in Fig. 16. The attempt is to capture the effect of the ratio of shear capacity and flexure resistance on the response of structural elements for varying blast scenarios and accordingly identify the failure mode.

It is envisaged from Figs. 16 and 17 that with increased V_o/R_m, response shifts towards the "quasi-static zone", ductile behavior of the structure can be observed. In the impulsive zone, we observe shear failure (brittle failure), with increased V_o/R_m ratio for a given beam, we can move

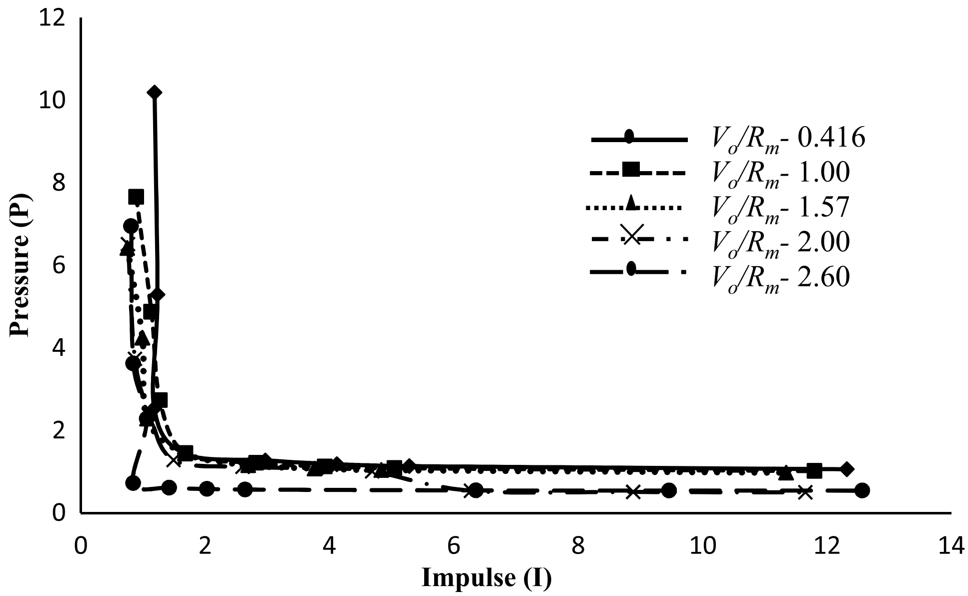

Fig. 16 Pressure-Impulse diagram using coupled SDOF system for variable V_o/R_m ratio

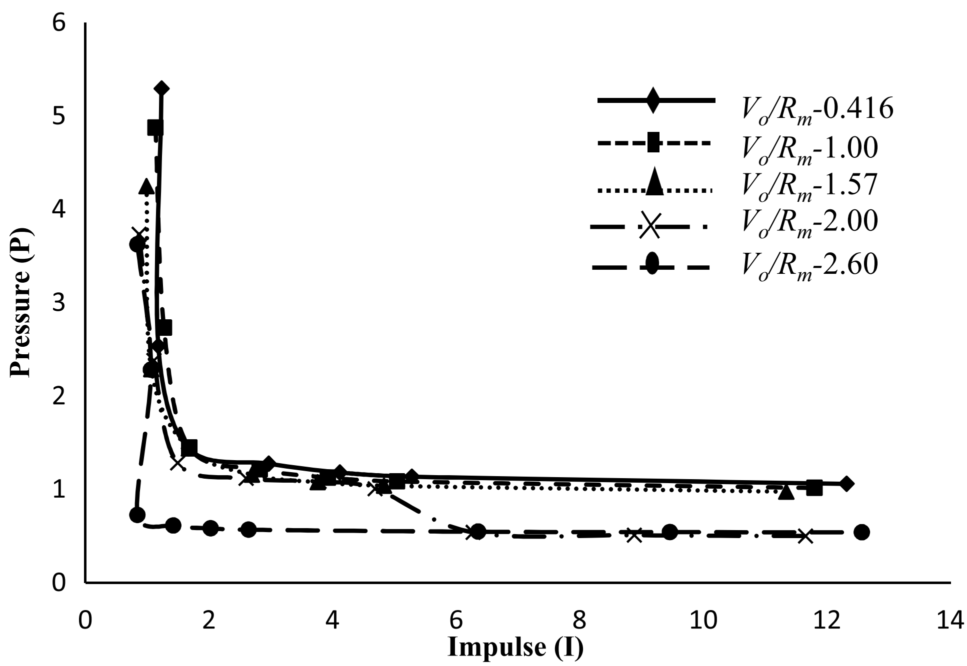

Fig. 17 A dynamic regime of Pressure-Impulse diagram using coupled SDOF system

our failure zone from brittle shear failure towards ductile flexure failure.

Conclusion

The response of the structure or structural part subjected to blast load has been obtained in the form of a P-I curve by including the contribution of higher modes through the application of the superposition approach and Coupled SDOF approach.

Higher modes significantly influence the response of a structural element against blast load, as is clear from the results derived in the form of Pressure-Impulse (iso-damage) curves. It should be observed that these iso-damage (P-I) curves for the blast in the dynamic and impulsive regime are very different from those derived using the traditional SDOF paradigm.

Using Timoshenko beam theory including higher modes, traditional SDOF approach and Coupled SDOF approach, comparison research was conducted to examine the variance in response of a structure subjected to blast load. The P-I curve obtained using the traditional SDOF approach and Timoshenko beam theory considering first mode display convergence, while the curve obtained using the Coupled SDOF approach converges with that obtained using Timoshenko beam theory including higher modes. The response of the structure in the form of Pressure-Impulse curves obtained using various aforementioned approaches is heavily influenced by flexibility. The Pressure-Impulse curve obtained moves towards the non-conservative side (quasi-static regime) as flexibility of structural element decreases. The effect of shear-flexure capacity (V_o/R_m) ratio is also studied for Coupled SDOF approach. As (V_o/R_m) ratio increases for a beam, the response shifts towards quasi-static regime for the given blast load case, indicating ductile (flexure) behavior.

In the event of a near-field explosion, higher modes (flexure and shear) are understandably important. The current analysis demonstrates that the formulation of Timoshenko produces an accurate response regardless of the structure's flexibility. The Coupled SDOF technique is a viable alternative for achieving response for varied blast ranges without experimenting with number of modes parameter in a much simplified way.

Author contributions Anita Bhatt wrote the main manuscript text and prepared all figures reported in manuscript. Pradeep Bhargava provided valuable guidance. All authors reviewed the manuscript.

Funding The authors declare that no funds, grants, or other support were received during the preparation of manuscript.

Declarations

Conflict of interest On behalf of all authors, the corresponding author declares that there is no conflict of interest regarding the publication of this manuscript.

Ethical approval On behalf of all authors, the corresponding author declares that we have followed the accepted principles of ethics at study, and there are no financial or personal conflicts of interest that might have impacted the study reported in this publication.

Human and animal rights No animal or human subjects were used in this work. This manuscript is an original paper and has not been published in other journals. We also confirm that there is no way our manuscript is in possible conflict with the ethical standards required by the journal.

References

Abedini, M., Mutalib, A. A., Baharom, S., & Hao, H. (2013). Reliability analysis of P-I diagram formula for RC column subjected to blast load. In *Proceedings of World Academy of Science, Engineering and Technology* (vol. 7 no. 8, pp. 253–257)

Abedini, M., Mutalib, A. A., Raman, S. N., Alipour, R., & Akhlaghi, E. (2019). Pressure-impulse (P–I) diagrams for reinforced concrete (RC) structures. *Archives Computational Methods Engineering., 26*, 733.

Bhatt, A., Bhargava, P., & Maheshwari, P. (2021). Contribution of higher modes in the dynamic response of reinforced concrete member subjected to blast IOP Conference Series. *Earth and Environment Sciences, 871*, 012003. https://doi.org/10.1088/1755-1315/871/1/012003

Bhatt, A., Bhargava, P., & Maheshwari, P. (2023). Coupled SDOF system approach for reinforced concrete beams subjected to blast loading. *Engineering Structures, 22*, 4435 (under communication)

Biggs, J. M. (1964). Introduction to Structural Dynamics. *Mc Graw Hill Book Company*. https://doi.org/10.1007/978-3-7091-2656-1_2

Campidelli, M., & Viola, E. (2007). An analytical-numerical method to analyze the single degree of freedom models under air blast loading. *Journal of Sound and Vibration, 302*(1–2), 260–286. https://doi.org/10.1016/j.jsv.2006.11.024

Chopra, A. K. (2012). *Dynamics of structures*. Prentice Hall 4th edition

Cormie, D., Mays, C., & Smith, P. (2009). *Blast effects on buildings* (2nd ed.). Thomas Telford Ltd.

Department of Defense, UFC 3–340–02. (2008). *Structures to resist the effects of the accidental explosions*. Technical Report, Unified Facilities Criteria

Dragos, J., & Wu, C. (2014). Interaction between direct shear and flexural responses for blast loaded one-way reinforced concrete slabs using a finite element model. *Engineering Structures, 72*, 193–202. https://doi.org/10.1016/j.engstruct.2014.04.043

Fallah, A. S., & Louca, L. A. (2007). Pressure-impulse diagrams for elastic-plastic-hardening and softening single-degree-of-freedom models subjected to blast loading. *International Journal of Impact Engineering, 34*(4), 823–842. https://doi.org/10.1016/j.ijimpeng.2006.01.007

Gantes, C. J., & Pnevmatikos, N. G. (2004). Elastic-plastic response spectra for exponential blast loading. *International Journal of Impact Engineering, 30*(3), 323–343. https://doi.org/10.1016/S0734-743X(03)00077-0

Han, S. M., Benaroya, H., & Wei, T. (1999). Dynamics of transversely vibrating beams using four engineering theories. *Journal of Sound and Vibrations, 225*(5), 935–988. https://doi.org/10.1006/jsvi.1999.2257

Ibrahim, Y. E., Ismail, M. A., & Nabil, M. (2017). Response of Reinforced Concrete Frame Structures under Blast Loading. *Procedia Engineering, 171*, 890–898. https://doi.org/10.1016/j.proeng.2017.01.384

Jayasooriya, R. (2010). Vulnerability and damage analysis of reinforced concrete framed buildings, PhD thesis

Jones, N., & Alves, M. (2004). Post-failure motion of beams under blast loads. *Structural Materials, 15*, 3–12.

Kadid, A. (2008). Stiffened plates subjected to uniform blast loading. *Journal of Civil Engineering and Management, 14*(3), 155–161. https://doi.org/10.3846/1392-3730.2008.14.11

Krauthammer, T. (2008). Pressure-impulse diagrams and their applications. *In Modern Protective Structures, Civil and Environmental Engineering*. https://doi.org/10.1201/9781420015423.ch8

Krauthammer, T., Astarlioglu, S., Blasko, J., Soh, T. B., & Ng, P. H. (2008). Pressure-impulse diagrams for the behavior assessment of structural components. *International Journal of Impact Engineering, 35*(8), 771–783. https://doi.org/10.1016/j.ijimpeng.2007.12.004

Li, Q. M., & Meng, H. (2002). Pulse loading shape effects on pressure–impulse diagram of an elastic-plastic, single-degree-of-freedom structural model. *Journal of Engineering Mechanics ASCE, 44*, 1985–1998.

Liu, L., Zong, Z., Tang, B., & Li, M. (2018). Damage Assessment of an RC Pier under Noncontact Blast Loading Based on P - I Curves. *Shock and Vibration*. https://doi.org/10.1155/2018/9204036

Ngo, T., Mendis, P., Gupta, A., & Ramsay, J. (2007). Blast loading and blast effects on structures - An overview. *Electronic Journal of Structural Engineering, 7*, 76–91.

Ross, T. J. (1986). Impulsive direct shear failure in RC slab. *Journal of Structural Engineering ASCE, 1*, 1661–1677.

Shi, H., Salim, H., & Ma, G. (2012). Using P-I diagram method to assess the failure modes of rigid-plastic beams subjected to triangular impulsive loads. *International Journal of Protective Structures, 3*(3), 333–353. https://doi.org/10.1260/2041-4196.3.3.333

Slawson, B. T. R. (1984). *Dynamic shear failure of shallow-buried flat-roofed reinforced concrete structures subjected to blast loading*. Technical Report SL-84–7 Structures Laboratory US Army Waterways Experiment Station, Vicksburg, MS.

Smith, P. D., & Hetherington J. G. (1994). *Blast and ballistic loading of structures*. CRC Press

Syed, Z. I., Liew, M. S., Hasan, M. H., & Venkatesan, S. (2014). Single-degree-of-freedom based pressure-impulse diagrams for blast damage assessment. *Applied Mechanics and Materials, 567*, 499–504. https://doi.org/10.4028/www.scientific.net/AMM.567.499

Van Der Meer, L. J., Kerstens, J. G. M., & Bakker, M. C. M. (2010). P-I diagrams for linear-elastic cantilevered Timoshenko beams including higher modes of vibration. *Heron, 55*(1), 51–83.

Wu, C. (2012). Research Development on Protection of Structures against Blast Loading at the University Of Adelaide. *Australian Journal of Structural Engineering, 13*(1), 97–109. https://doi.org/10.7158/13287982.2012.11465102

Xu, J., Wu, C., & Li, Z. X. (2014). Analysis of direct shear failure mode for RC slabs under external explosive loading. *International Journal of Impact Engineering, 69*, 136–148. https://doi.org/10.1016/j.ijimpeng.2014.02.018

Youngdahl, C. K. (1970). Correlation parameters for eliminating the effect of pulse shape on dynamic plastic deformation. *Journal of Applied Mechanics Transactions ASME, 37*(3), 744–752. https://doi.org/10.1115/1.3408605

Yu, R., Zhang, D., Chen, L., & Yan, H. (2018). Non-dimensional pressure–impulse diagrams for blast-loaded reinforced concrete beam-columns referred to different failure modes. *Advances of Structural Engineering, 21*(14), 2114–2129. https://doi.org/10.1177/1369433218768085

Zhang, C., Gholipour, G., & Mousavi, A. A. (2019). Nonlinear dynamic behavior of simply-supported RC beams subjected to combined impact-blast loading. *Engineering Structures, 181*, 124–142. https://doi.org/10.1016/j.engstruct.2018.12.014